Journal of Diabetes Science and Technology
Volume 2, Issue 6, November 2008

SYMPOSIUM

Percutaneous Window Chamber Method for Chronic Intravital Microscopy of Sensor–Tissue Interactions

Heidi E. Koschwanez, M.Sc.,[1] Bruce Klitzman, Ph.D.,[1,2] W. Monty Reichert, Ph.D.[1]

Abstract

Background:

A dorsal, two-sided skin-fold window chamber model was employed previously by Gough in glucose sensor research to characterize poorly understood physiological factors affecting sensor performance. We have extended this work by developing a percutaneous one-sided window chamber model for the rodent dorsum that offers both a larger subcutaneous area and a less restrictive tissue space than previous animal models.

Method:

A surgical procedure for implanting a sensor into the subcutis beneath an acrylic window (15 mm diameter) is presented. Methods to quantify changes in the microvascular network and red blood cell perfusion around the sensors using noninvasive intravital microscopy and laser Doppler flowmetry are described. The feasibility of combining interstitial glucose monitoring from an implanted sensor with intravital fluorescence microscopy was explored using a bolus injection of fluorescein and dextrose to observe real-time mass transport of a small molecule at the sensor–tissue interface.

Results:

The percutaneous window chamber provides an excellent model for assessing the influence of different sensor modifications, such as surface morphologies, on neovascularization using real-time monitoring of the microvascular network and tissue perfusion. However, the tissue response to an implanted sensor was variable, and some sensors migrated entirely out of the field of view and could not be observed adequately.

Conclusions:

A percutaneous optical window provides direct, real-time images of the development and dynamics of microvascular networks, microvessel patency, and fibrotic encapsulation at the tissue–sensor interface. Additionally, observing microvessels following combined bolus injections of a fluorescent dye and glucose in the local sensor environment demonstrated a valuable technique to visualize mass transport at the sensor surface.

J Diabetes Sci Technol 2008;2(6):977-983

Author Affiliations: [1]Department of Biomedical Engineering, Duke University, Durham, North Carolina and [2]Kenan Plastic Surgery Research Labs, Duke University Medical Center, Durham, North Carolina

Abbreviations: (E-collar) Elizabethan collars, (LDF) laser Doppler flowmetry, (nA) nanoamperes, (NIH) National Institutes of Health, (PLLA) poly-L-lactic acid

Keywords: glucose sensor, microcirculation, PLLA, porous, window chamber

Corresponding Author: W. Monty Reichert, Ph.D., Duke University, Department of Biomedical Engineering, 136 Hudson Hall, Box 90281, Durham, NC 27708; email address reichert@duke.edu

Introduction

For decades, window chamber models have been used to nondestructively visualize cellular phenomena in living tissue.[1–3] The use of these chambers for glucose sensor research was pioneered by Gough.[4–6] Window chambers can be used for days to months in an animal,[5] permitting long-term, serial investigations of microcirculation, wound healing, and cellular interactions. Window chambers, such as the dorsal skin fold model,[4,7,8] have been employed in a number of species, including hamsters, mice, rats, and rabbits,[6,9–12] and have been used to monitor tumor growth,[9,10] biomaterial interactions,[11,13,14] and tissue remodeling around implantable sensors.[1–3] Many of these windows provide only a limited separation distance (typically 200 μm or less) between the two transparent plates, making the observed tissues relatively two dimensional.

Percutaneous window models expose implanted sensors to a larger subcutaneous area than afforded by traditional "two-dimensional" skin-fold models, allowing a more realistic sensor–tissue interaction. This article describes procedures for implanting a percutaneous acrylic window, as well as performing intravital microscopy and laser Doppler flowmetry (LDF) to evaluate microcirculation and red blood cell perfusion in tissue adjacent to an implanted sensor. Specifically, sensors with and without porous poly-L-lactic acid (PLLA) coatings were implanted beneath the windows to demonstrate the utility of this model in observing real-time changes at the sensor–tissue interface. It is well established that textured/porous surface morphologies of appropriate morphology will promote angiogenesis and reduce capsule thickness compared with smooth surfaces.[15–21]

To further understand the interplay among neovascularization, vessel patency, fibrotic encapsulation, and long-term sensor performance, a pilot study was performed to incorporate the window chamber model with real-time interstitial glucose monitoring. Several examples of the model's utility to observe and quantify changes in neovascularization at the sensor surface are discussed throughout this article, in addition to technical challenges and recommendations. Medtronic MiniMed SOF-SENSOR™ glucose sensors, MiniLink™ monitoring units, MiniLink™ chargers, MiniMed Com-Station™, and MiniLink™ transmitter software (Version 1.0A) were generously supplied by Medtronic MiniMed (Northridge, CA).

Materials and Methods

Rats

Male Sprague–Dawley type (CD) rats (150–200 grams, Charles River Laboratories, Inc., Wilmington, MA) were used for the percutaneous dorsal window chamber studies. All National Institutes of Health (NIH) guidelines for the care and use of laboratory animals (NIH Publication #85-23 Rev. 1985) were observed. Approval for these studies was granted by the Duke University Institutional Animal Care and Use Committee prior to initiation of the studies. Four rats were used to demonstrate the implantation and microscopic characterization methods.

Porous Coating and Sensor Preparation

Noncytotoxic, porous PLLA coatings with ~30-μm pores were constructed using the ammonium bicarbonate salt leaching/gas foaming technique of Nam and colleagues.[22] Details of the porous coating fabrication and nonfunctional sensor preparation have been published previously.[21] Nonfunctional sensors (plastic hub and glucose oxidase removed) were used to investigate the effects of porosity on tissue response. Functional sensors were used in the pilot study, which combined continuous glucose monitoring with intravital microscopy.

Anesthesia

Rats were anesthetized with 2.5% isoflurane (Baxter Healthcare Corp., Deerfield, IL) in oxygen at a flow of 1 liter/min, which was adjusted to effect after induction for window chamber implantation, intravital microscopy, and LDF. Each time the rats were anesthetized, Puralube® ocular lubricant (Pharmaderm, Melville, NY) was applied to each eye to prevent corneal drying.

Window Chamber Model

The surgical procedure was adapted from the rodent mammary window model of Shan and associates.[10] The dorsal skin was shaved, and a 10-mm-diameter circle was marked approximately 2 cm below the scapular region. The skin was cleaned with chlorhexidine (Baxter-Healthcare, Co. Deerfield, IL) and alcohol. A 10-mm-diameter circular full-thickness incision was performed and the skin was removed. Blunt dissection was used to form a shallow pocket around excised tissue to assist in fitting the acrylic window (15 mm diameter, 0.75 mm thick, with 10–12 holes drilled around the window perimeter for suturing).

One nonfunctional sensor was positioned in the middle of the excised area and sutured at each end (out of the field of view) to anchor the device in place. Following sensor placement, the window was secured with 5-0 monofilament sutures (**Figure 1a**). The wound was cleaned gently with hydrogen peroxide, followed by antibiotic ointment (Target Corporation, Minneapolis, MN). Before the rat recovered from anesthesia, 1 mg of flunixin meglumine (Fort Dodge Animal Health, Fort Dodge, IA) in 0.2 ml saline was administered subcutaneously remote from the optical window.

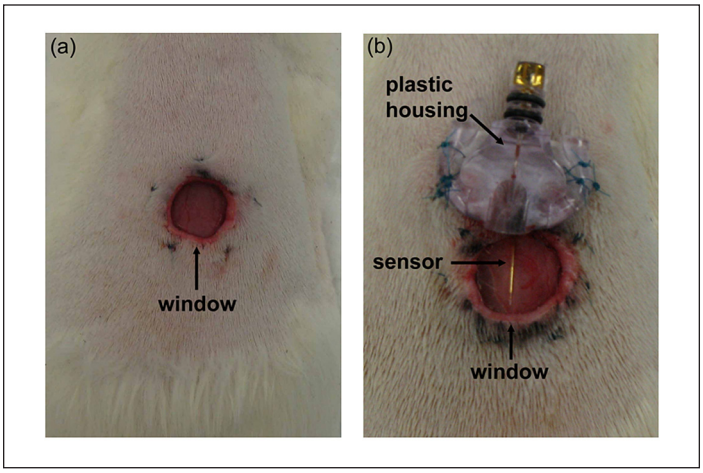

Figure 1. (a) Percutaneous window chamber **(b)** with Medtronic MiniMed SOF-SENSOR™ implanted percutaneously beneath window.

Rats were monitored daily for infection and to ensure that the window was still implanted. Additionally, antibiotic ointment was applied daily to the window area and rats were allowed access to rat chow and water *ad libitum*.

Laser Doppler Flowmetry

Following window implantation, and on days 3, 7, 10, and 14, capillary blood perfusion was measured noninvasively via laser Doppler flowmetry using the LaserFlo® BPM2 blood perfusion monitor (Vasamedics, Inc., St. Paul, MN). A fiber-optic needle probe was used noninvasively for all measurements. With the 680-nm wavelength laser diode and a fiber spacing of 200 μm, this laser Doppler flowmeter receives the majority of its signal from microvessels approximately 0.5 to 1.5 mm below the surface, although less signal is contributed by more superficial and deep microvessels.

Prior to taking measurements, the window surface was first cleaned with sterile saline. The needle-like fiber-optic probe was positioned directly adjacent to the sensor and lowered until the probe gently contacted the window with no microvessel compression. Six locations adjacent to the sensor, six locations within the window area, and five locations on the rat dorsum were sampled for blood perfusion flow at each time point per rat. After a 20-second signal stabilization period, the lowest flow observed over the subsequent 10 seconds was recorded in LDF units.

Intravital Microscopy

Intravital microscopy was performed immediately following LDF measurements. Microvessels around the sensors were imaged using a Leitz Laborlux 12 ME ST fluorescence microscope (Leica, Inc., Rockleigh, NJ), a 6.3× objective (Carl Zeiss, Inc., Thornwood, NY), a 75-watt xenon arc lamp (Osram GmbH, Augsburg, Germany), a fluorescein filter set (excitation 450–490 nm, emission ≥515 nm), and a Nikon CoolPix 5400 digital camera. This optical system resulted in an empirically determined functional depth of field of approximately 100 μm and a typical observation depth of approximately 100 μm. A Deltaphase isothermal pad (Braintree Scientific Inc., Braintree, MA) was placed on the microscope stage to maintain the rodent temperature at 37°C during imaging. While under anesthesia, 10 mg of sodium fluorescein (Sigma-Aldrich, St. Louis, MO) in 0.1 ml sterile saline was injected via the tail vein in a bolus. A minimum of four locations along the sensor and four locations within the window were captured. Microvessel length density and diameter were quantified off-line.

Window Care

After sacrifice on day 14, windows were excised carefully. Windows were cleaned first with a soft brush using mild antibacterial soap (Steris Corporation, Mentor, OH), followed by a 24-hour soak in soapy water, a 24-hour soak in 70% ethanol, and then ethylene oxide sterilized. Following sterilization, windows were degassed for at least 1 week before implantation.

Image Analysis

Total microvessel length and diameter. Images were opened in Image J 1.37a software (NIH, Bethesda, MD). The MeasureCumulativeDistances macro was downloaded and installed from the NIH Image J Web site to provide cumulative distance measurements along the length of a microvessel (segmented line). Two 1 × 1-mm^2 boxes were drawn digitally in each of the four sensor and four window images captured: boxes for the sensor images were drawn adjacent to the sensor–tissue interface. Boxes for the window images were drawn at least 1 mm from the sensor to prevent cross-counting of the vessels. A maximum of eight boxes adjacent to the sensor surface

and eight boxes within the window field were analyzed for vessel length and vessel diameter. Each vessel within the digital 1-mm^2 box was traced using the "segmented line selections" tool in the Image J package, followed by recording the sum of the accumulated lengths measured per box. The total microvessel length per mm^2 was calculated for each treatment group. Average microvessel diameter was also measured within each 1-mm^2 box per treatment group.

Combining Continuous Glucose Monitoring with Intravital Microscopy

Preoperative preparations

Rats were acclimated to wearing Elizabethan collars (E-collar) for 18–48 hours prior to surgery. Prior to surgery, rats were lightly anesthetized to shave the dorsal region and to remove the E-collar. Rats were then fitted with a rat jacket (Harvard Apparatus, Holliston, MA) (**Figure 2**) containing the shell of a Medtronic MiniLink™ unit and sensor and allowed to move unrestrained in their cage. The MiniLink unit (~5 grams, 3.5 × 3 × 1 cm) powered the glucose sensor, collected glucose data, and transmitted data using radio frequency to the computer for analysis.

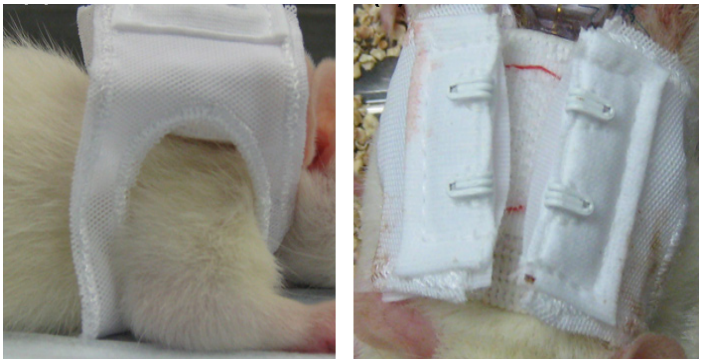

Figure 2. (a) Side view of rat jacket on an anaesthetized rat; **(b)** top view of rat wearing jacket.

Rats were observed carefully to assess optimal placement of the window and sensor. The location where the base of the sensor shaft rested on the rat's dorsum was marked while the rat was in a neutral, resting position. Placing the window or sensor directly between scapulae was avoided to minimize sensor damage and possible discomfort for the rat.

Surgery

A 10-mm-diameter circle was drawn approximately 2 mm below the mark for sensor placement (i.e., window center was 7 mm below sensor insertion point). The dorsum was scrubbed repeatedly with chlorhexidine and alcohol. Flunixin meglumine (1 mg) was injected subcutaneously. A 10-mm circular dorsum incision was performed, followed by blunt dissection around the perimeter of the excised tissue. The wound was flushed with sterile saline and dried with sterile gauze.

A pilot hole for sensor insertion was created 2 mm proximal to the excised tissue by puncturing the dermis with a 19-gauge needle. A functional Medtronic MiniMed SOF-SENSOR was introduced through the pilot hole. The sensor was aligned down the center of the window area (**Figure1b**), and the sensor and acrylic disk were sutured in place.

Laser Doppler flowmetry was then performed, followed by hydrogen peroxide cleaning around the window perimeter and antibiotic application. The E-collar was fastened and the rat was returned to its cage. Every 24 to 48 hours, the E-collars were removed for 0.5 to 2 hours to allow the rats to groom.

Sensor Testing

Rats were anesthetized with isoflurane to remove the E-collar, clean the window, and dress the rat with the rat jacket. The MiniLink unit was connected to the sensor and secured to the jacket using an in-house fabricated Velcro pouch. Once connected to the sensors, units were initialized for 2 hours before sensor data were collected. While anesthetized, blood flow was measured through the window within 1 mm of the sensor surface and at random locations within the window area. Rat motion was not restricted by the rat jackets or MiniLink unit, allowing the rats to groom during the 2-hour system initialization period.

Following the 2-hour initialization period, the rats were again anesthetized. Two to three tail vein pricks were performed to test the baseline glucose concentration. A 25-gauge butterfly syringe was inserted into the tail vein and secured. Once the sensor beneath the window was in focus for imaging, 0.5 ml of 50% dextrose with 20 mg/ml fluorescein was injected at 0.1 ml/min. Concomitantly, a video was captured to analyze tissue perfusion at the sensor–tissue interface to correlate with real-time glucose sensor data collected by the MiniLink unit.

Rats were imaged for approximately 30 minutes, with video recordings for the first 3 to 10 minutes, and still images were taken at 10-minute intervals. An additional image was taken after 1–2 hours postbolus injection. The MiniLink unit and jacket were then removed, the E-collar replaced, and antibiotic ointment applied to the window area before the rat was returned to its cage.

Glucose–Fluorescein Bolus Imaging Analysis

Average electrical current values [nanoamperes (nA)], corresponding to the local interstitial glucose concentration at the sensor surface, were downloaded from the MiniLink. Downloaded data were plotted in GraphPad Prism software. Video and images acquired were processed in Image J to correlate increases in glucose concentration with fluorescence intensity at the sensor surface and at various distances normal to the surface over the experiment time course.

Results and Discussion

The time interval most confounding to sensor performance occurs during the first 2 weeks following implantation[21,23] when sensors commonly experience highly variable or dramatically reduced sensor signals. The effects of acute inflammation and tissue dynamics that hinder sensor reliability have been observed after the fact using histological methods that provide only tissue snapshots at experiment termination. While information about collagen deposition and microvessel density around a sensor can be gleaned from histological analysis, little is known about real-time tissue dynamics or microvascularization patency using this method. The percutaneous window chamber model was developed to better characterize the response of the tissue and its effects on signals recorded from implanted glucose sensors.

Porous-coated Medtronic MiniMed glucose sensors were used to demonstrate how this model can be used to image and characterize changes in microvascular architecture to two distinctly different sensor surfaces. These porous coating were reported previously to induce a 3-fold increase in vessel density per mm^2 compared with unmodified (smooth surface) MiniMed glucose sensors after 3 weeks in the rat subcutis, based on histological analysis.[21] **Figure 3** shows the dramatic difference in tissue response that was observed using this model between a sensor with a smooth surface **(a)** and a sensor with a porous coating **(b)**. While both images were taken 10 days postsensor/window implantation, a nearly 4-fold difference in blood perfusion and a 10-fold difference in vascularity were observed. Laser Doppler flowmetry at day 10 yielded an average perfusion of 48 ± 9 LDF units (mean ± SEM) adjacent to the smooth surface implants and 196 ± 59 LDF units adjacent to the porous surface implants. The total microvessel length (mm microvessels per mm^2) adjacent to the smooth surface was 1.1 ± 0.7 mm/mm^2, whereas the microvessel length adjacent to the porous surface was 11.0 ± 0.7 mm/mm^2.

The host response to the acrylic window was accounted for by implanting control window chambers to examine tissue response to the window material in the absence of a sensor (**Figure 3c**). Preliminary analysis of the control window suggested that observed differences between porous and smooth surface morphologies were not influenced by the presence of the acrylic window. On day 10, total microvessel length was 2.4 ± 1.1 mm/mm^2 and average perfusion was 109 ± 12 LDF for the control window.

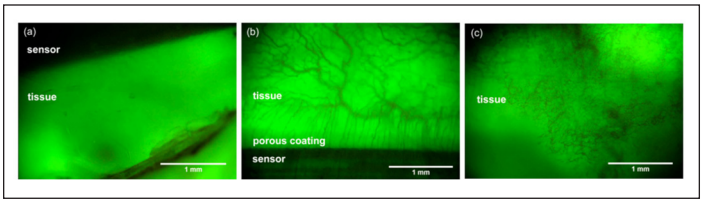

Figure 3. Day 10 neovascularization **(a)** at the unmodified (smooth) sensor–tissue interface, **(b)** at the porous coated sensor–tissue interface, and **(c)** beneath the control window.

The two primary criteria for defining a blood microvessel were (1) length of structure greater than diameter (to minimize counting dark areas as vessels) and (2) good contrast between the dark vessel structure and the green fluorescent tissue. Because hemoglobin strongly absorbs light between 525 and 580 nm, the microvessels appear dark against the fluorescent tissue.[24,25] Variability in light intensity was substantial over the entire image, which prevented using a simple analysis based on a threshold of intensity. Additional criteria for determining if a structure was a microvessel included observing branched structures stemming from the structure of interest or if the structure of interest was a branch from a structure that met the vessel criteria.

Infusing a mixed bolus of dextrose and fluorescein provided a protocol to directly compare both visual and sensor measurements of mass transport at the sensor surface. The technique was demonstrated by imaging a rat with an unmodified MiniMed sensor on day 3. As demonstrated in **Figure 4**, the fluorescein–glucose bolus injection allowed (1) real-time images of fluorescein perfusion through the tissue toward the sensor surface, (2) continuous monitoring of the changing glucose concentration in the local sensor environment, and (3) comparison of time lag between tissue perfusion and sensor response.

Prior to the bolus injection (**Figure 4a**, $t = 0$), no fluorescein was present in the tissue and the baseline sensor signal was 18.5 nA. Over the next 3 minutes (**Figures 4b–4d**), tissue fluorescence intensity increased steadily and

capillaries became visible as fluorescein initially perfused the capillaries and then leaked into the tissue. Nonfluorescent tissue outlining the sensor suggested that perfusion immediately adjacent to the sensor had not occurred. This observation was corroborated with sensor current, which had not increased from baseline until 5 minutes after the injection began (**Figure 4g**). At 30 minutes, fluorescein had perfused the tissue adjacent to the sensor, eliminating the sensor outline (**Figure 4e**). The glucose sensor current indicated that a peak sensor response occurred approximately 20 minutes postinjection. Fluorescein takes approximately 24 hours to clear,[26] resulting in intense tissue fluorescence after 110 minutes (**Figure 4f**). This is in contrast to the glucose clearance and consumption that were observed, which led to a return to baseline sensor current within approximately 50 minutes. Image processing techniques will be combined with changes in fluorescence intensities to characterize the mass transport phenomena surrounding the sensor with respect to time and distance from the sensor.[27,28]

The optical window technique demonstrated several difficulties. First, we observed considerable variability in the host tissue response to an implanted sensor from rat to rat. Second, sensor migration beneath the window was substantial in some rats, which may have been due to animal movement and/or loosening of sutures anchoring the sensor. In most cases, gentle manipulation of the dorsal dermis permitted window repositioning over the migrated sensor. Typically, sensor migration occurred during the first 24 to 48 hours postimplantation, after which tissue integration prevented further sensor migration. Third, sensor motion from animal respiration was minimized for laser Doppler readings and for intravital microscopy by attaching the LDF probe to a ring stand and capturing microscopic images at the end of expiration. Fourth, exudate accumulation beneath the window prevented optimal focusing. Resolution was improved by aspirating the accumulated exudate with a syringe inserted several millimeters away from the window to prevent bleeding under the window.

Finally, window infection was minimized by daily topical application of antibiotics around the window perimeter. Antibiotics were not applied to the subcutaneous tissue adjacent to the sensor, and it is unlikely that antibiotics would diffuse from the site of application on the skin adjacent to the edge of the window to the viewing area, as that would require traversing through the stratum corneum, through the epidermis, through the dermis, and laterally several millimeters to the site of the sensor observation.

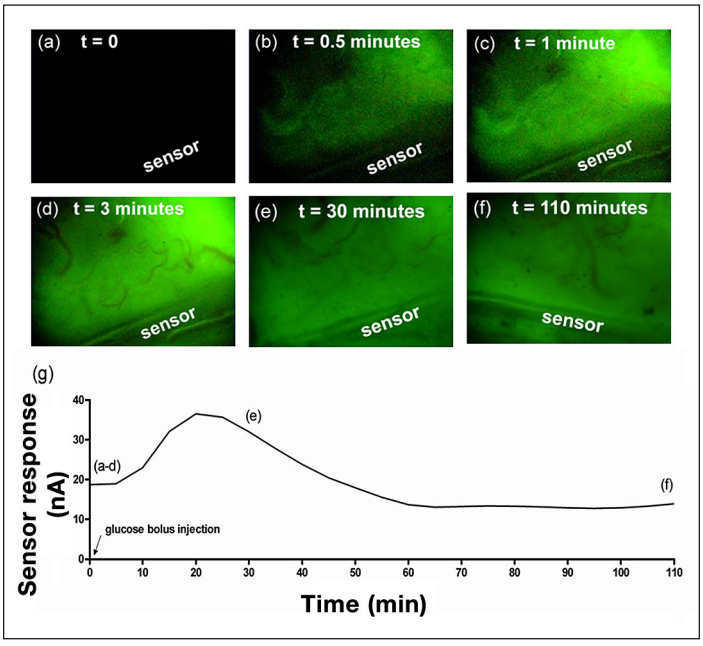

Figure 4. Progression of the dextrose–fluorescein bolus in the tissue surrounding the SOF-SENSOR at Day 3: **(a)** at t = 0 min, the tissue is void of fluorescein; **(b)** at t = 0.5 min, a green glow beneath window, though not yet adjacent to the sensor; **(c)** at t = 1 min; **(d)** at t = 3 min, the fluorescein intensity increases; **(e)** at t = 30 min, the sensor barely visible from fluorescein perfusion; **(f)** at t = 110 min, the glucose has cleared, but the fluorescein has not; and **(g)** the continuous sensor response (nA) to the dextrose–fluorescein bolus.

Conclusions

The percutaneous window chamber model permits real-time noninvasive examination of tissue remodeling adjacent to an implanted sensor. Histology provides only a snapshot of vascularization and/or fibrotic encapsulation at the sensor–tissue interface, whereas this model offers repeated nondestructive quantification of complex tissue–sensor interactions over time. Our studies demonstrated consistent differences in tissue perfusion and neovascularization between smooth and porous coatings. Combining intravital microscopy with continuous glucose monitoring using this model enables quantification of mass transport around glucose sensors and comparison of coatings. However, variability between rats and migration of the sensors continue to present challenges to this promising technique.

Funding:

Funding was provided by NIH DK054932, Medtronic, Inc.

Acknowledgements:

The authors thank Drs. Lori Norton and Mark Dewhirst for helpful discussions and Dr. Siqing Shan for the acrylic windows. The authors gratefully acknowledge Medtronic MiniMed for the donation of sensors, software, and equipment and for the use of clean room space, as well as financial support. Special thanks to Victor Giron, Neil Heil, and Drs. Larry Wang, Rajiv Shah, and John Mastrototaro for their kind help and generosity.

Disclosure:

Presented work was partially funded by Medtronic, Inc.

References:

1. Vajkoczy P, Ullrich A, Menger MD. Intravital fluorescence videomicroscopy to study tumor angiogenesis and microcirculation. Neoplasia. 2000;2(1-2):53-61.
2. Menger MD, Laschke MW, Vollmar B. Viewing the microcirculation through the window: some twenty years experience with the hamster dorsal skinfold chamber. Eur Surg Res. 2002;34(1-2):83-91.
3. Makale M. Intravital imaging and cell invasion. Methods Enzymol. 2007;426:375-401.
4. Ertefai S, Gough DA. Physiological preparation for studying the response of subcutaneously implanted glucose and oxygen sensors. J Biomed Eng. 1989;11(5):362-8.
5. Makale MT, Chen PC, Gough DA. Variants of the tissue-sensor array window chamber. Am J Physiol Heart Circ Physiol. 2005;289(1):H57-65.
6. Makale MT, Lin JT, Calou RE, Tsai AG, Chen PC, Gough DA. Tissue window chamber system for validation of implanted oxygen sensors. Am J Physiol Heart Circ Physiol. 2003;284(6):H2288-94.
7. Makale MT, Lin JT, Calou RE, Tsai AG, Chen PC, Gough DA. Tissue window chamber system for validation of implanted oxygen sensors. Am J Physiol Heart Circ Physiol. 2003;284(6):H2288-94.
8. Papenfuss HD, Gross JF, Intaglietta M, Treese FA. Transparent access chamber for the rat dorsal skin fold. Microvasc Res. 1979;18(3):311-8.
9. Sorg BS, Moeller BJ, Donovan O, Cao Y, Dewhirst MW. Hyperspectral imaging of hemoglobin saturation in tumor microvasculature and tumor hypoxia development. J Biomed Optics. 2005;10(4):44004.
10. Shan SQ, Sorg B, Dewhirst MW. A novel rodent mammary window of orthotopic breast cancer for intravital microscopy. Microvasc Res. 2003;65(2):109-17.
11. Menger MD, Walter P, Hammersen F, Messmer K. Quantitative analysis of neovascularization of different PTFE-implants. Eur J Cardiothorac Surg. 1990;4(4):191-6.
12. Algire GH. An adaptation of the transparent chamber technique to the mouse. J Natl Cancer Inst. 1943;4:1-11.
13. Laschke MW, Haufel JM, Thorlacius H, Menger MD. New experimental approach to study host tissue response to surgical mesh materials *in vivo*. J Biomed Mater Res A. 2005;74(4):696-704.
14. Laschke MW, Witt K, Pohlemann T, Menger MD. Injectable nanocrystalline hydroxyapatite paste for bone substitution: *in vivo* analysis of biocompatibility and vascularization. J Biomed Mater Res B Appl Biomater. 2007;82(2):494-505.
15. Ward WK, Slobodzian EP, Tiekotter KL, Wood MD. The effect of microgeometry, implant thickness and polyurethane chemistry on the foreign body response to subcutaneous implants. Biomaterials. 2002;23(21):4185-92.
16. Brauker JH, Carrbrendel VE, Martinson LA, Crudele J, Johnston WD, Johnson RC. Neovascularization of synthetic membranes directed by membrane microarchitecture. J Biomed Mater Res. 1995;29(12):1517-24.
17. Sharkawy AA, Klitzman B, Truskey GA, Reichert WM. Engineering the tissue which encapsulates subcutaneous implants. II. Plasma-tissue exchange properties. J Biomed Mater Res. 1998;40(4):586-97.
18. Marshall AJ, Irvin CA, Barker T, Sage EH, Hauch KD, Ratner BD. Biomaterials with tightly controlled pore size that promote vascular in-growth. Abstracts of Papers of the American Chemical Society 2004 Aug;228:U386.
19. Updike SJ, Shults MC, Gilligan BJ, Rhodes RK. A subcutaneous glucose sensor with improved longevity, dynamic range, and stability of calibration. Diabetes Care. 2000;23(2):208-14.
20. Gilligan BC, Shults M, Rhodes RK, Jacobs PG, Brauker JH, Pintar TJ, Updike SJ. Feasibility of continuous long-term glucose monitoring from a subcutaneous glucose sensor in humans. Diabetes Technol Ther. 2004;6(3):378-86.
21. Koschwanez HE, Yap FY, Klitzman B, Reichert WM. *In vitro* and *in vivo* characterization of porous poly-L-lactic acid coatings for subcutaneously implanted glucose sensors J Biomed Mater Res A. 2008 Jan 15.
22. Nam YS, Yoon JJ, Park TG. A novel fabrication method of macroporous biodegradable polymer scaffolds using gas foaming salt as a porogen additive. J Biomed Mater Res. 2000;53(1):1-7.
23. Updike SJ, Shults MC, Rhodes RK, Gilligan BJ, Luebow JO, von Heimburg D. Enzymatic glucose sensors. Improved long-term performance *in vitro* and *in vivo*. ASAIO J. 1994;40(2):157-63.
24. Altshuler GB, Yaroslavsky I. Absorption characteristics of tissues as a basis for the optimal wavelength choice in photodermatology. Burlington, MA: Palomar Medical Technologies, Inc.; 2004.
25. Van Assendelft OW. Spectrophometry of haemoglobin derivatives. Springfield, IL; Assen, The Netherlands: Thomas; Royal Vangorcum Ltd.; 1970.
26. O'Goshi KI, Serup J. Safety of sodium fluorescein for *in vivo* study of skin. Skin Res Technol. 2006;12(3):155-61.
27. Dreher MR, Liu W, Michelich CR, Dewhirst MW, Yuan F, Chilkoti A. Tumor vascular permeability, accumulation, and penetration of macromolecular drug carriers. J Natl Cancer Instit. 2006;98(5):335-44.
28. Wu NZ, Klitzman B, Rosner G, Needham D, Dewhirst MW. Measurement of material extravasation in microvascular networks using fluorescence video-microscopy. Microvasc Res. 1993;46(2):231-53.